ISSN 0021-3640, JETP Letters, 2022, Vol. 116, No. 5, pp. 288–292. © Pleiades Publishing, Inc., 2022.
ISSN 0021-3640, JETP Letters, 2022. © Pleiades Publishing, Inc., 2022.

OPTICS
AND LASER PHYSICS

Numerical Simulation of GaAs/AlO_x High Index Contrast Subwavelength Gratings for GaAs-Based Vertical Cavity Surface Emitting Lasers

Y. Luo[a] and Y.-Q. Hao[a, *]

[a] *National Key Lab of High-Power Semiconductor Lasers, Changchun University of Science and Technology, Changchun, 130022 People's Republic of China*

**e-mail: hyq72081220@aliyun.com*

Received June 14, 2022; revised August 1, 2022; accepted August 2, 2022

A GaAs/AlO_x high index contrast subwavelength grating with TE polarization is presented for the GaAs-based vertical cavity surface emitting laser (VCSEL). The rigorous coupled wave analysis (RCWA) method is employed to simulate the dependence between its reflection characteristics and grating parameters. Especially, the effects of the stress buffer layer, shape errors, and angle of incidence on refractivity are also analyzed in detail. The high index contrast subwavelength grating has a large reflection bandwidth up to 97 nm with good polarization selectivity, and exhibits large tolerance in preparation, which makes it easier to integrate with the VCSEL. What's more, its sensitivity to angle of incidences facilitates the single-mode VCSELs' implement.

DOI: 10.1134/S0021364022601154

Vertical cavity surface emitting laser (VCSEL) is widely used in many applications because of their superior performances, such as low threshold current, small divergence angle, circular beam profile, two-dimensional array configuration and low power consumption [1–5]. Nowadays, VCSELs are attracting more attentions in the fields of free space optical communication, optical information processing, all-optical communication and laser pumping [6–9]. However, VCSEL has some defects, such as multimode operation and unstable polarization, which seriously affect its actual performance. Therefore, some methods were introduced in order to improve its mode and polarization properties. Polarization in VCSELs can be controlled given polarization-dependent gain/loss regions in VCSELs, such as surface relief [10], external-cavity feedback [11], and subwavelength grating [12]. Also, high index contrast subwavelength grating (HCG) attracts attention for its ability to control both mode and polarization.

The period of subwavelength grating is less than the incident wavelength, so there is only zero order diffraction. The predominant characteristic of a HCG is that the fringes of high index grating are completely surrounded by low index medium (generally air or silicon dioxide), which forms a large index difference. By adjusting the grating material, thickness, duty cycle and other parameters, its reflectivity can reach more than 99%. It can be used to replace the P-type distributed Bragg reflectors (DBRs) of a VCSEL, which can greatly reduce the series resistance and absorption loss of the device. The HCG mirror can not only decrease the thickness of VCSEL, but also fix polarization. In 2004 [13], Michael C. Y. Huang et al. reported a subwavelength grating with very broad reflection spectrum. Their work presented its potential application in VCSEL. Three years later, they demonstrated for the first time a VCSEL integration with HCG [14]. The HCG is composed of freely suspended periodic stripes of $Al_{0.6}Ga_{0.4}As$ with air as the low-index sublayer. In 2010, Vadim Karagodsky et al. analyzed the ultra-high reflectivity feature of subwavelength dielectric gratings [15]. They explained the origin of ~100% reflectivity of HCG. In 2020 [16], Åsa Haglund and Tien-Chang Lu jointly developed the first electrically injected GaN-based VCSEL with TiO_2 HCG.

The typical HCG for VCSEL based on GaAs is mostly composed of GaAs/air or Si/SiO_2 [14, 17]. The suspended GaAs/air HCG has some disadvantages, such as complicated fabrication process and poor mechanical stability, while for the HCG with Si/SiO_2 it is difficult to achieve a precise control of its thickness. GaAs/AlO_x HCG for a mid-infrared VCSEL based on GaSb has been proposed in [18, 19]. However, a metamorphic growth deteriorates the HCG performance, and the device laser operation couldn't be observed because of a lack of reflectivity of HCG [19]. The GaAs/AlO_x HCG with the same material system as the half-VCSEL can be integrated with

VCSEL through one-time epitaxial technology, which is of great significance to obtain high quality wafers. Furthermore, the low stress between HCG and the half-VCSEL is crucial to keep the long-term stability of the device. In order to match HCG with VCSEL perfectly, the reflectivity of HCG is numerically computed by rigorous coupled-wave analysis (RCWA). In addition, the influences of stress buffer layer, grating morphology and the incident light angle on reflectivity are studied in detail.

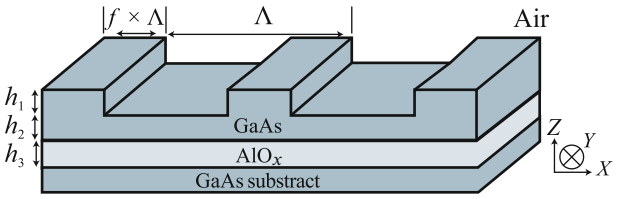

Fig. 1. (Color online) Schematic diagram of HCG: period Λ, fill factor f, grating layer h_1, stress buffer layer h_2, low index sublayer h_3.

HCG MIRROR DESIGN

Figure 1 shows the schematic diagram of a HCG, including grating layer, stress buffer layer and low index sublayer. HCG is composed of GaAs and AlO_x. The AlO_x as the low index sublayer ($n \approx 1.6$) may be obtained from AlAs by oxidation. The large index difference between the AlO_x and GaAs grating layer ($n \approx 3.538$) will be beneficial to increase the width of the reflection band. Due to a large index contrast and near-wavelength dimensions, there exists a wide wavelength range where only two modes have real propagation constants in the z-direction. The two modes carry similar energy but opposite phases at the HCG output plane, thus causing destructive interference. Finally, the transmission is canceled and all of the energy must be reflected [20]. To improve the stability of the HCG, the GaAs layer is not completely etched to form the grating layer and the stress buffer layer.

HCG belongs to subwavelength grating, and its equivalent index and energy band structure are different in different polarization modes, so it can be designed as a mirror with polarization. If a HCG is chosen as the mirror of a VCSEL to replace the conventional DBRs, the polarization mode with larger threshold gain will be suppressed and the other with smaller threshold gain will emit. The diffraction efficiency of subwavelength grating can be calculated by RCWA. The diffraction efficiencies corresponding to reflection and transmission can be expressed respectively as follows [21]:

$$D_{ri} = |R_{s,i}|^2 \mathrm{Re}\left(\frac{k_{\mathrm{I},zi}}{k_0 n_{\mathrm{I}} \cos\theta}\right) + |R_{p,i}|^2 \mathrm{Re}\left(\frac{k_{\mathrm{I},zi}/n_{\mathrm{I}}^2}{k_0 n_{\mathrm{I}} \cos\theta}\right), \quad (1)$$

$$D_{ti} = |T_{s,i}|^2 \mathrm{Re}\left(\frac{k_{\mathrm{II},zi}}{k_0 n_{\mathrm{I}} \cos\theta}\right) + |T_{p,i}|^2 \mathrm{Re}\left(\frac{k_{\mathrm{II},zi}/n_{\mathrm{II}}^2}{k_0 n_{\mathrm{I}} \cos\theta}\right), \quad (2)$$

where, i is the diffraction order, θ is the angle of incidence, k_0 is the incident wave vector, n_{I}, n_{II} are the indexes of the incident region and the transmission region, $k_{\mathrm{I},zi}$, $k_{\mathrm{II},zi}$ are the wave vectors along the Z-axis in the incident region and the transmission region. $R_{s,i}$ and $T_{s,i}$ correspond to intensity of reflection and transmission for TE mode respectively, and $R_{p,i}$, $T_{p,i}$ are for the TM mode. It can be seen that the reflectivity of the grating is not only related to the TE and TM components of the incident light, but also related to the angle of incidence θ and parameters of the grating. Therefore, the reflectivity can be improved at the corresponding wavelength by optimizing relevant parameters.

The HCG is set for 940 nm GaAs-based VCSELs with TE polarization, so it should have more than 99.5% reflectivity for the TE mode, meanwhile keeping the TM mode reflectivity below 90% at around 940 nm. In our simulation, the incident light is perpendicular to the surface of the low index sublayer. Considering the feasibility of preparation, the HCG should not only exhibit good performance, but also have large manufacturing tolerance. So, we will discuss the effects of the grating parameters, topography errors and angle of incidence on reflectivity in detail.

RESULTS AND DISCUSSIONS

The diffraction order of the grating is directly related to the grating period and the incident wavelength. It can be seen from Fig. 2 that the grating period determines the location of the center wavelength on the high reflection band, and the high reflection band moves towards longer wavelength with the increase in the grating period. Since the HCG is used for VCSEL, it is necessary to avoid other high order diffractions except zero order. As can be seen from Fig. 3, only zero order diffraction exists around the central wavelength when the period is 0.78 μm, and the reflection efficiency is even close to 100%. As shown in the inset, there is almost no energy transmitted through the gratings, which is a double-mode destructive interference phenomenon [15]. Figure 4 shows that there is a broad high reflectivity band when the period is in the range of $0.702 \sim 0.87$ μm. The period can be controlled accurately by lithographic method; thus, the mirror can be precisely fabricated.

Fill factor and grating thickness determine the reflectivity and bandwidth [13]. Figure 5 shows the effect of fill factor and grating thickness. The fill factor appropriate range is 17.5–38.6%, which provides a large tolerance for fabrication. According to the interference conditions among the Bloch modes, the grating thickness is the most important factor affecting the

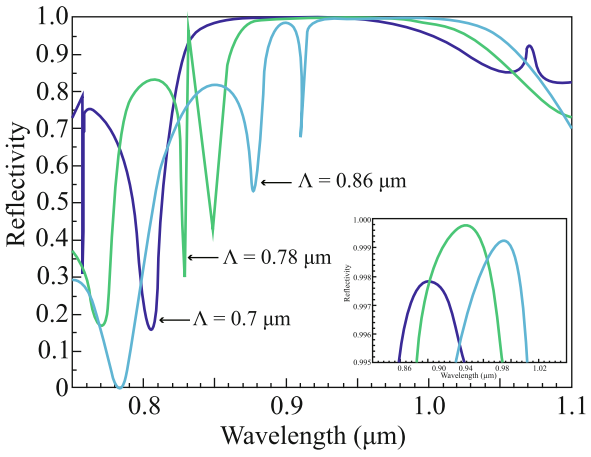

Fig. 2. (Color online) Reflectivity versus the wavelength and period. The inset shows reflectivity exceeding 99.5% for the TE mode.

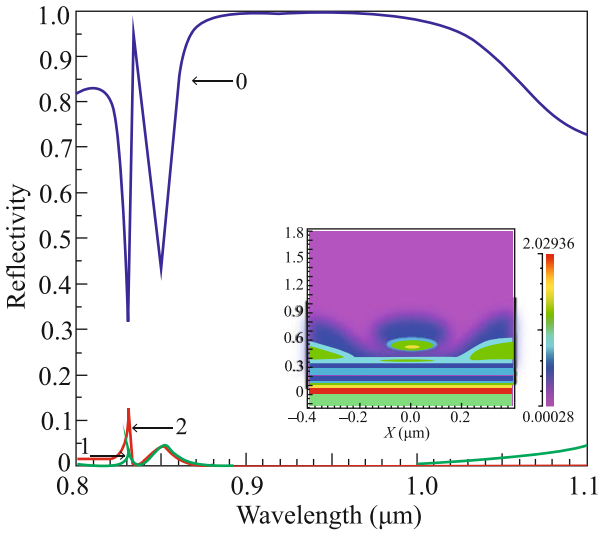

Fig. 3. (Color online) Reflection spectra corresponding to different diffraction orders with a period of 0.78 μm and the inset shows electric field intensity distribution.

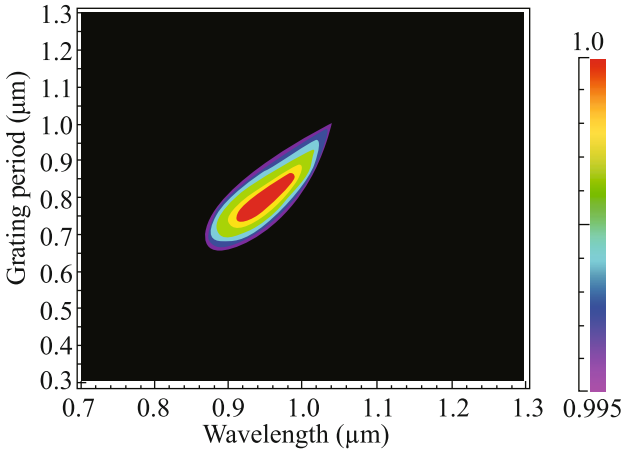

Fig. 4. (Color online) Reflectivity versus the period for the TE mode.

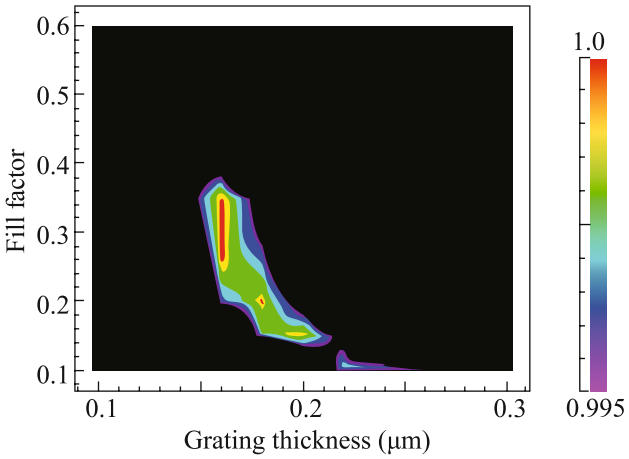

Fig. 5. (Color online) Reflectivity versus the fill factor and grating thickness for the TE mode.

reflectance. As can be seen, although the high reflection band is particularly sensitive to the change of h_1, the HCG still exhibits a broad high reflection band when grating thickness is in range of $0.15 \sim 0.182$ μm. Its shallow depth and large tolerance are undoubtedly very good for fabricating.

It's worth noting that a stress buffer layer introduced in HCG to improve the stress problem caused by oxidation shrinkage affects the reflectivity. Figure 6a shows its effects on the reflection of the grating. The high reflection band changes periodically with the increase in the stress buffer layer thickness. The layer is selected in the range of $0.132 \sim 0.221$ μm according to central wavelength, high reflection bandwidth and epitaxial technology. As shown in Fig. 6b, the low index sublayer has little effect on the high reflection. The HCG always has a wide band of high reflection around central wavelength when h_3 is above 46 nm. Here the range of h_3 is chosen as $0.14 \sim 0.22$ μm.

Figure 7a shows the reflectivity spectrum of TE-HCG with ideal rectangular shape. It can be seen that the high reflection band is located at $0.888 \sim 0.985$ μm and $\Delta\lambda/\lambda_0 = 10\%$, with its TE reflectivity more than 99.5% and the TM reflectivity lower than 90%. TE-HCG has the advantages of large period, small fill factor and shallow groove depth, which can greatly reduce the difficulty of its fabrication. The above results are based on the model of rectangular

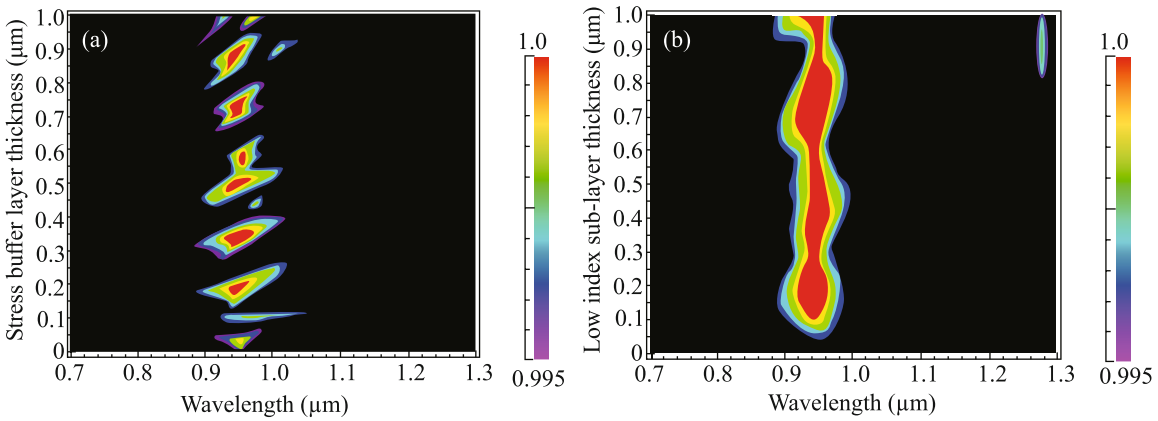

Fig. 6. (Color online) Reflectivity versus the wavelength and grating parameters: (a) stress buffer layer thickness; (b) low index sublayer thickness.

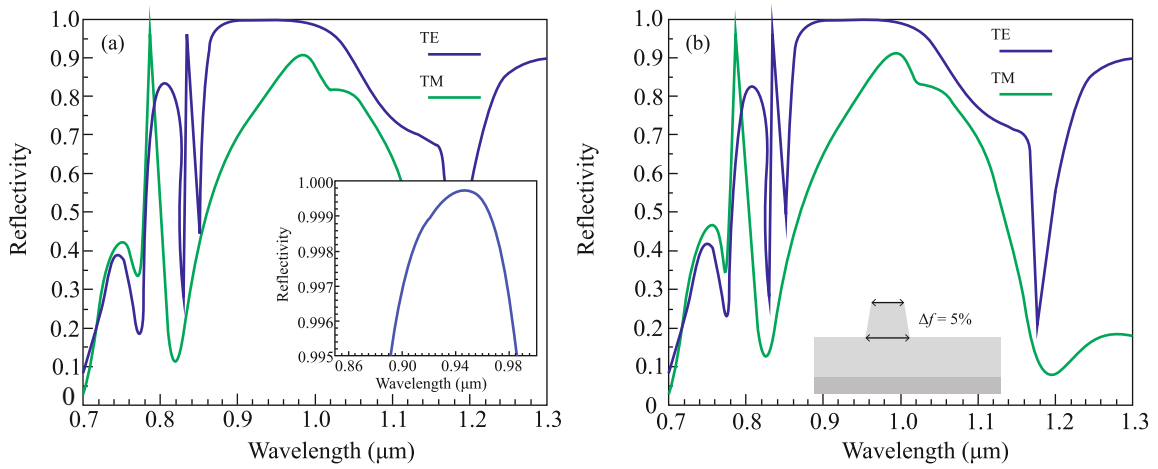

Fig. 7. (Color online) Reflectivity spectra of the TE-HCG. (a) Rectangular grating ($\Lambda = 0.781$ μm, $h_1 = 0.166$ μm, $h_2 = 0.189$ μm, $h_3 = 0.17$ μm, $f = 25.4\%$). (b) Trapezoidal grating ($\Lambda = 0.781$ μm, $h_1 = 0.166$ μm, $h_2 = 0.189$ μm, $h_3 = 0.17$ μm, $f_{upper} = 25.4\%$, $f_{lower} = 29.2\%$.

grating. However, the perpendicularity of grating sidewall will be affected by mask shape and etching conditions in actual processing, and the actual grating is usually of a trapezoidal shape. Therefore, we considered the influence of grating shape on reflectivity. As shown in Fig. 7b, although there is 5% difference between the upper and lower fill factors, the trapezoidal TE-HCG has a little deterioration in the shape of its high reflection band, the central wavelength moves towards the long-wavelength by 10 nm, and high reflection bandwidth still keeps 96 nm. This greatly reduces the difficulty of fabrication and deterioration of the mirror performance. Figure 8 shows that the HCG reflectivity is sensitive to the angle of incidence. When the angle of incidence is 3°, the highest reflectivity of TE mode is already as low as 95%. Therefore, a VCSEL integrated with such a HCG will behave good in the single-mode operation, and the other

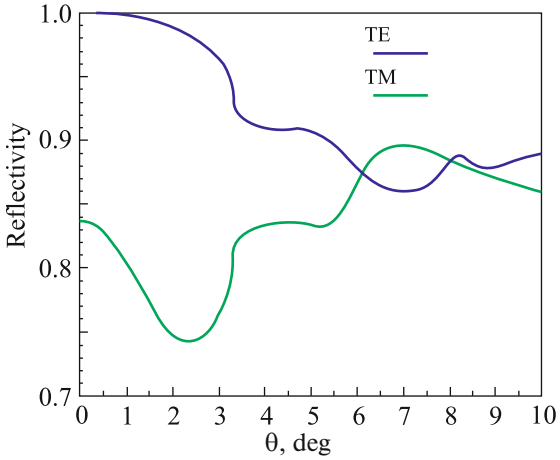

Fig. 8. (Color online) Reflectivity versus the angle of incidence.

higher-order modes will be suppressed for their divergence.

CONCLUSIONS

Based on the RCWA method, a GaAs/AlO_x TE-HCG mirror for GaAs-based VCSEL is simulated and investigated numerically. The results show that the fill factor and grating thickness are the most critical parameters, because they determine the reflectivity and bandwidth. Furthermore, the stress buffer layer also affects the reflection properties of the HCG, whose high reflection band changes periodically with the buffer thickness. However, there is only a little deterioration in the shape of high reflection band even if the fill factor difference between the upper and lower of the grating is up to 5%. Therefore, the GaAs/AlO_x HCG not only makes it easier to integrate with VCSEL, but also can effectively avoid the deterioration of its reflection performance. Moreover, it can be prepared with less difficulty due to its large period, shallow etching depth and large morphology tolerance. Meanwhile, its sensitivity to the angle of incidences is good for VCSEL to operate with single-mode. The HCG has a large reflection bandwidth up to 97 nm at around 940 nm ($\Delta\lambda/\lambda_0 = 10\%$) with its TE reflectivity more than 99.5% and TM reflectivity lower than 90%. VCSEL integrated with HCG will undoubtedly have the characteristics of smaller size, single mode, and polarization stability. It can match perfectly the tunable diode laser absorption spectroscopy for gas detection.

CONFLICT OF INTEREST

The authors declare that they have no conflicts of interest.

REFERENCES

1. Z. Zhen-Bo, X. Chen, X. Yi-Yang, Z. Kang, L. Fa, and S. Guang-Di, Chin. Phys. B **21**, 3 (2012).
2. P. S. Yeh, C. C. Chang, Y. T. Chen, D. W. Lin, J. S. Liou, C. C. Wu, J. H. He, and H. C. Kuo, Appl. Phys. Lett. **109**, 24 (2016).
3. Md. Jarez, K. V. Kalosha, B. Dieter, J. Pohl, and M. Weyers, Opt. Express **24**, 26 (2016).
4. W. Zhen-fu, N. Yong-qiang, Z. Yan, S. Jingjing, Z. Xing, Z. Lisen, W. Wei, L. Di, H. Yongsheng, C. Haibing, L. Qin, L. Yun, and W. Lijun, Opt. Express **18**, 23 (2010).
5. W. Xiao-fa, W. Zheng-mao, and X. Guang-qiong, Acta Phys. Sin. **65**, 2 (2016).
6. L. Rui, W. Li-ping, P. Fang-wei, Y. Hao-yu, and L. Chun-jing, J. Quant. Econ. **35**, 1 (2018).
7. B. Kelleher, M. Dillane, and E. A. Viktorov, Light Sci. Appl. **10**, 1 (2021).
8. C. Chih-Hsien, S. Chih-Chiang, K. Hsuan-Yun, H. Dan-Hua, W. Huai-Yung, Y. Yen-Wei, L. Yun-Ting, C. Sung-Wen Huang, T. Cheng-Ting, C. Yu-Chieh, K. Tsung Sheng, W. Chao-Hsin, K. Hao-Chung, L. Po-Tsung, and L. Gong-Ru, Opto-Electron. Adv. **1**, 3 (2018).
9. S. O. Slipchenko, A. A. Podoskin, V. S. Golovin, P. S. Gavtina, V. V. Shamkhox, D. N. Nikolaev, V. V. Zolotarev, N. A. Pikhtin, T. A. Bagaev, M. A. Ladugin, A. A. Marmalyuk, and V. A. Simakov, IEEE Trans. Electron Dev. **67**, 1 (2020).
10. L. Shuo, G. Bao-lu, S. Guo-zhu, and G. Xia, Acta Phys. Sin. **61**, 18 (2012).
11. Z. Tong, J. Zhi-wei, W. An-bang, H. Yan-hua, W. Long-sheng, G. Yuan-yuan, and W. Yun-cai, IEEE Photon. Technol. Lett. **33**, 7 (2021).
12. Z. Xiang-wei, N. Yong-qiang, Q. Li, L. Yun, and W. Li-jun, Chin. J. Lumin. **34**, 11 (2013).
13. C. F. R. Mateus, M. C. Y. Huang, Y. Deng, A. R. Neureuther, and C. J. Chang-Hasnain, IEEE Photon. Technol. Lett. **16**, 2 (2004).
14. M. C. Y. Huang, Y. Zhou, and C. J. Chang-Hasnain, Nat. Photon. **1**, 119 (2007).
15. K. Vadim, F. G. Sedgwick, and C. J. Chang-Hasnain, Opt. Express **18**, 16 (2010).
16. C. Tsu-Chi, H. Ehsan, H. Kuo-bin, B. Jörgen, G. Johan, H. Åsa, and L. Tien-chang, ACS Photon. **7**, 4 (2020).
17. C. Chevallier, N. Fressengeas, F. Genty, and J. Jacquet, J. Opt. **13** (2011).
18. W. Huang-ming, M. Wen-qin, H. Jin, G. Ding-shan, H. Ran, J. Hong, G. Rui-min, W. Wen-hua, and Z. Zhi-ping, J. Opt. **12**, 045703 (2010).
19. Y. Laaroussi, C. Chevallier, F. Genty, N. Fressengeas, L. Cerutti, T. Taliercio, O. Gauthier-Lafaye, P. F. Calmon, B. Reig, and J. Jacquet, Opt. Mater. Express **3**, 1576 (2013).
20. R. Yi, Y. Weijian, C. Chase, M. C. Y. Huang, D. P. Worland, S. Khaleghi, M. R. Chitgarha, M. Ziyadi, A. E. Willner, and C. J. Chang-Hasnain, IEEE J. Sel. Top. Quantum Electron. **19**, 4 (2013).
21. Y. Hui, Z. Jin, W. Xiao-wei, and H. Xing-fan, Chin. J. Lasers **29**, 9 (2002).